Neurosci. Bull. February, 2023, 39(2):194–212
https://doi.org/10.1007/s12264-022-00898-7

www.neurosci.cn
www.springer.com/12264

ORIGINAL ARTICLE

miR-34b-3p Inhibition of eIF4E Causes Post-stroke Depression in Adult Mice

Xiao Ke[1,2] · Manfei Deng[1,2] · Zhuoze Wu[3] · Hongyan Yu[1,2] · Dian Yu[1,2] · Hao Li[1,2] · Youming Lu[2,4] · Kai Shu[5] · Lei Pei[1,2]

Received: 23 February 2022 / Accepted: 14 May 2022 / Published online: 8 July 2022

Abstract Post-stroke depression (PSD) is a serious and common complication of stroke, which seriously affects the rehabilitation of stroke patients. To date, the pathogenesis of PSD is unclear and effective treatments remain unavailable. Here, we established a mouse model of PSD through photothrombosis-induced focal ischemia. By using a combination of brain imaging, transcriptome sequencing, and bioinformatics analysis, we found that the hippocampus of PSD mice had a significantly lower metabolic level than other brain regions. RNA sequencing revealed a significant reduction of miR34b-3p, which was expressed in hippocampal neurons and inhibited the translation of eukaryotic translation initiation factor 4E (eIF4E). Furthermore, silencing eIF4E inactivated microglia, inhibited neuroinflammation, and abolished the depression-like behaviors in PSD mice. Together, our data demonstrated that insufficient miR34b-3p after stroke cannot inhibit eIF4E translation, which causes PSD by the activation of microglia in the hippocampus. Therefore, miR34b-3p and eIF4E may serve as potential therapeutic targets for the treatment of PSD.

Keywords Post-stroke depression · Hippocampus · miRNA · Microglia · Neuroinflammation

Introduction

Post-stroke depression (PSD), one of the sequelae of stroke, severely affects the functional outcome of stroke survivors and is associated with high mortality. The clinical features of PSD include depressed mood, diminished interest, delayed thinking, and sleep disorder [1–4]. The incidence of PSD is 25%–76%, and 45.4% of depression cases occur within 1 month after stroke, and 91.8% of these are mild to moderate [5–9]. Depression seriously affects treatment motivation, compliance, and self-rehabilitation, which in turn increase the disability rate and mortality [9–11]. Therefore, the prognosis of stroke is closely related to the severity of PSD. Early identification and intervention for PSD are beneficial to the prognosis of stroke patients [11, 12]. The treatment of PSD is based on symptomatic support therapies, but there is no effective drug at present. Current theories on the pathogenesis of PSD involve neuroanatomy, neurotransmitters, the neuroendocrine system, the inflammatory response, neurotrophic factors, neuropeptides, and social psychological factors [13–18]. However, the molecular mechanisms have not yet been fully elucidated.

Supplementary Information The online version contains supplementary material available at https://doi.org/10.1007/s12264-022-00898-7.

✉ Lei Pei
peilei@hust.edu.cn

1 Department of Neurobiology, School of Basic Medicine, Tongji Medical College, Huazhong University of Science and Technology, Wuhan 430030, China

2 The Institute for Brain Research, Collaborative Innovation Center for Brain Science, Huazhong University of Science and Technology, Wuhan 430030, China

3 Department of Pathophysiology, Basic Medical School, North Sichuan Medical College, Nanchong 637100, China

4 Department of Physiology, School of Basic Medicine, Tongji Medical College, Huazhong University of Science and Technology, Wuhan 430030, China

5 Department of Neurosurgery, Tongji Hospital, Tongji Medical College, Huazhong University of Science and Technology, Wuhan 430030, China

Epigenetics is closely related to the occurrence of PSD, and it mainly regulates the development of ischemic stroke through DNA methylation, histone modification, and post-transcriptional regulation of miRNAs [19, 20]. MicroRNAs (miRNAs), a major class of non-coding RNAs with a length of ~22 nucleotides are integrated into the RNA-induced silencing complex and bind to the 3′-UTR (untranslated region) of the target mRNA, which can induce down-regulation of target transcript expression through mRNA degradation or the inhibition of translation, and finally regulate gene expression [21, 22] and participate in important biological processes such as cell proliferation, apoptosis, differentiation, neurodevelopment, and other life activities by acting on the corresponding target genes [22, 23]. MiRNAs are widely expressed in the brain and play a key role in the pathophysiology of various neurological diseases such as stroke, schizophrenia, and depression [24]. By using RNA sequencing (RNA-seq) and bioinformatics analysis, our previous study revealed 778 genes increasingly expressed in the brain of mice with stroke [25]. And normal expression of miRNA maintains physiological functions of nervous system and homeostasis, which is associated with synaptic plasticity, neural development, and neural differentiation. While low miRNAs expression is linked with neuronal degeneration, the inflammatory response, and oxidative stress [26]. Whether and how the altered miRNAs and genes function in the occurrence and development of PSD is still unclear.

In this study, we selected and confirmed a mouse model of PSD by light-induced cortical ischemia and unsupervised fuzzy clustering analysis with various behavioral tests. Furthermore, we revealed a novel molecular mechanism by brain imaging and RNA-seq, and investigated a possible treatment strategy for PSD.

Materials and Methods

Animals

C57BL/6J male mice at 3 months of age were bred and reared in the animal facilities under the same conditions in accordance with the institutional guidelines of the Animal Care and Use Committee of Huazhong University of Science and Technology within the University' s animal care facility, in plastic cages in an air-conditioned room at 24°C under a 12 h light-dark cycle (lights on at 08:00) and food and water *ad libitum*. Mice were group-housed at 3–5 per cage before experiments. Mice with left cortical ischemia were housed individually to mimic social isolation during the experiments. All behavioral tests were carried out during the light phase of the cycle.

Photothrombosis Ischemia Model

We applied photothrombosis-induced focal ischemia following procedures similar to those described by Labat-gest *et al*. [27]. Briefly, mice were anesthetized with 5% chloral hydrate before surgery. The skull was exposed and a fiber-optic bundle mounted on a cold light source (φ = 1.5 mm, wavelength 560 nm, 150 W, aperture B2, 2750 K, KL 1500 LCD, Schott, Germany), was placed in close contact with the left skull surface with a focus at 1.4 mm posterior to the bregma and 3 mm lateral to the midline (left anterior cortex). The photosensitive dye rose Bengal (Sigma-Aldrich 632-69-9) was dissolved in sterile saline to a concentration of 15 mg/mL and was injected intraperitoneally (10 μL/g body weight). Then, after ~5 min to allow the dye to diffuse and enter the blood stream, we started 15 min of focal illumination of the skull to ensure that the photothrombotic lesion was located in the left anterior cortical layers without injuring the adjacent or subcortical areas. Next, the incisions were sutured and the mice were housed individually to mimic social isolation. We used sham-operated animals as controls, which were subjected to the same procedure except for light irradiation.

Selection Criteria for Sample Screening Before Behavioral Tests

The selection criteria for the sample screening were as follows, first, assessment of the general health of mice to exclude any gross abnormalities (such as poor coat appearance with bald patches or sores, blood encrusted around the body, labored breathing, low body weight, abnormal body temperature, hypo-activity in the home cage, absence of nest-building, hypersensitivity to handling, circling, and even tremors, seizures, or other easily-observed abnormalities) that might influence any behavioral testing; second, behaviors related to gross neurological functions (such as wild-running, hunching while walking, and excessive grooming or freezing) were evaluated in an empty cage environment; and last but not least, simple and quick tests of neurological reflexes (such as eye blink, ear twitch, whisker twitch, and the righting reflex) were applied sequentially in every mouse.

Behavioral Tests

The behavioral tests were selected to cover a range of accepted classic models of depression, and were applied ~1 month after cerebral ischemia [28]. All behavioral tests were conducted in an enclosed and quiet lab room with constant light, temperature, and humidity between 08:00 and 18:00. Videos were recorded using ETHO-Vision (Noldus) and analyzed using Any-maze by the same experimenter blinded to

the experimental protocol. Mice that received more than one behavioral test had at least 24 h of rest between tests and no mice were given the same test twice.

Assessment of Exploratory Behavior

Exploratory behavior was assessed in a two-way shuttle avoidance box placed in a dark, soundproof and airy cabinet. This box was a rectangular chamber (60 cm × 30 cm × 30 cm) divided by a non-transparent partition with a small (8 cm × 10 cm) channel connecting two adjacent cubicle-shaped compartments of equal size. The metal grille floor of the compartment was a weight-sensitive sensor that sensed and conveyed information about the mouse's activity to a computerized data acquisition system to control the conditioned stimulus (sound from a speaker on the celling of the compartment) and the electric shock delivery program (Techman, Chengdu, China). First, each mouse was placed in the chamber for adaptation and then allowed to freely explore both compartments for 5 min. If the mouse did not shuttle over to the other compartment after 3 min, the experimenter manually directed it through the channel. If the mouse failed to shuttle back 3 min later, the experimenter did the same as before. The voluntarily exploratory shuttles between compartments were recorded and counted by the experimenter.

Two-way Shuttle Avoidance Test

After completion of the exploratory behavioral assessment, mice were trained in a 50-trial two-way shuttle avoidance test. A training session consisted of 50 tracking conditioning trials. The conditional stimulus (CS) was a 10-s cue tone; the unconditional stimulus (US) was an electric shock (0.2 mA) for a maximum of 10 s after CS termination; The inter-trial interval (ITI) was 60 s. Mice could have the following responses, (1) Escape: mice shuttle to the adjacent compartment after the start of the US shock, the shock stops, and an ITI begins; (2) Escape-failure: mice do not move to the adjacent compartment, and the ITI begins after the end of the 5-s shock; or (3) Avoidance: mice shuttle to an adjacent compartment when a CS tone is heard, the tone stops, an ITI begins, and mice avoid the shock.

Sucrose Preference Test (SPT)

The SPT is a behavioral test of an animal's ability to experience pleasure, an impairment of which is an essential feature of depression. The SPT was applied in home cages equipped with two drinking bottles. Prior to the first test, all mice were subjected to 48 h of forced exposure to the 1% sucrose solution, the only liquid available for drinking, which was designed to habituate the mice to it. For the next 2 days mice were given a free choice between the bottles, one containing 1% sucrose and the other containing tap water. To prevent the effect of the bottle or its position on the drinking behavior, the experimenter switched the position of the bottle after 12 h. The consumption of water and sucrose solution was calculated by weighing the bottles. The preference for sucrose was expressed by calculating the amount of sucrose solution consumed as a percentage of the total liquid drunk {(Sucrose preference = Sucrose Intake (g)/[(Sucrose Intake (g) + Water Intake (g))] × 100}).

Open Field Test (OFT)

Mice were handled for 3 days. Then we measured locomotor activity in clear boxes (43.2 cm × 43.2 cm × 50 cm), outfitted with photo-beam detectors for monitoring horizontal and vertical activity [29]. Data were collected *via* a PC and were analyzed with MED Associates Activity Monitor Data Analysis software. Mice were placed in a corner of the open-field apparatus and left to move freely. Recorded variables were resting time (s), ambulatory time (s), vertical/rearing time (s), jump time (s), stereotypic time (s), and average velocity (cm/s). Mice were not exposed to the chamber prior to testing. Data were individually recorded for each mouse for 30 min.

Elevated Plus Maze (EPM)

The plus maze had two walled arms [closed arms: 35 cm (length) × 6 cm (width) × 22 cm (height) and two open arms: 35 cm (length) × 6 cm (width)]. The maze was elevated 74 cm from the floor. Each mouse was placed on the center section, allowed to freely explore the maze, and monitored with ImageEP software66. The time spent in the open *versus* closed arms during a 10-min period was recorded [29].

Forced Swimming Test (FST)

Mice were placed inside a vertical transparent glass cylinder 25 cm high with a diameter of 10 cm containing 15 cm of tap water maintained at 23–25°C and left there for 6 min, while only the last 4 min were scored for immobility by EthoVision XT 14. Each mouse was judged to be immobile when it ceased to struggle and remained floating motionless in the water, making only those movements that were necessary to keep its head above the water as previously described [30].

Tail Suspension Test (TST)

Each mouse was suspended within its own three-walled (white) rectangular compartment [45 cm (Height) × 15 cm (Width) × 15 cm (Depth)] in the middle of an aluminum suspension bar using adhesive tape, as previously described

[31]. The width and depth were such that the mouse could not touch the walls. The duration of the test is 6 min. EthoVision XT 14 was used to score the immobility during the last 4 min.

Cluster Analysis

To screen the post-stroke depression-like phenotype from all ischemic mice, unsupervised fuzzy clustering was applied based on a previous study [28]. Clustering can provide useful and reliable information by grouping the comprehensive behavioral data into different clusters, where the data are similar in each cluster. Similarity is defined by a distance metric, and the best partition of the data is obtained by using the elements of the membership matrix to define which cluster each data element belongs to. Thus, clustering evaluates the relationship between patterns in a dataset by organizing them into groups or clusters, so that patterns within a cluster are more similar than patterns belonging to other clusters. In this study, we analyzed the clusters based on the number of fuzzy points in each cluster and the hypervolume (determinant of clustering) of each cluster, with the former divided by the latter to give the cluster density.

TTC Staining and FJ Staining

The cerebral infarction and ischemic areas were also be determined by 2,3,5-triphenyltetrazolium chloride (TTC) staining. The brain was removed rapidly 24 h after ischemia, and frozen at −20°C for 30 min. Coronal slices (6 slices per mouse) were cut at 1 mm from the frontal tips, and immersed in 2% TTC (Sigma, CA, USA) at 37°C for 20 min in the dark. Subsequently, the presence of infarctions was determined by examining the area of negative TTC staining. Cell death was also assessed by FJ staining. Briefly, brain tissue slides were immersed for 3 min in 100% ethanol, for 1 min in 70% ethanol, and for 1 min in distilled water, and then incubated in a solution containing 0.01% Fluoro-Jade C (FJ; AG325, Millipore) and 0.1% acetic acid (1:10) for 30 min on a shaker. After three 10-min washes, the slides were cover-slipped and imaged with a laser-scanning confocal microscope (LSM 510, Carl Zeiss). The number of FJ-positive (FJ^+) cells in each group was counted.

RNA-Sequencing and Bioinformatics Analysis

MiRNA was isolated from mouse brain tissue using an RNAzol® RT RNA Isolation Reagent kit (Sigma-Aldrich) according to the manufacturer's protocol as previously described [26]. Three groups of mice were used and each group had three replicates. The library preparations and quality control of RNA-sequencing were performed by Novogene. The libraries were sequenced on a HiSeqTM2500 sequencer with 50-bp single-end sequencing run by Novogene. RNA-sequencing quality was assessed using FastQC (http://www.bioinformatics.babraham.ac.uk/projects/fastqc). The FastQC file was aligned to the latest mouse reference genomic sequence GRCm38.p6 using miRDeep2 [32] to identify known and unknown miRNAs. For the samples with replications, we applied DESeq2 [33] to the identification of differentially-expressed miRNAs for up- and down-regulation between each group. And we used a threshold of 0.05 to filter out the exponential component. To analyze Gene Ontology (GO) and pathway enrichment, we used enriched GO in the R package clusterProfiler (version 3.6.0) to identify the enriched biological process gene function terms. The significance of enriched GO terms was evaluated by a hypergeometric test with false discovery rate <0.05.

Reverse Transcription and Quantitative PCR

Total miRNA was isolated from micro-dissected hippocampus using an RNAzol® RT RNA Isolation Reagent kit (Sigma-Aldrich). A cDNA synthesis kit (Toyobo) was used for the reverse transcription reaction according to the manufacturer's instructions. We used 1 μg total miRNA. Samples were incubated for 5 min at 65°C. All samples were then added to a 5× mix, heated to 37°C for 15 min, and reactions were stopped by heating to 98°C for 5 min. These cDNA samples were then amplified using qPCR with different miRNA primers from Tiangen Biochemical Technology Co., Ltd. (Beijing. China) without disclosure of the proprietary primer sequences. The reactions were set up in duplicate in a total volume of 10 μL containing 5 μL of 2× miScript SYBR green PCR mix (GeneCopoeia, QP115) and 2 μL of template (1:5 dilution from the RT product) with a final concentration of 400 nmol/L of the primer. PCR was performed using a real-time PCR instrument (Cat# 1855201; Bio-Rad). The PCR cycle was as follows: 95°C/3 min, 40 cycles of 95°C/30 s, 60°C/45 s, and 95°C/1 min, and the melt-curve analysis was performed at the end of each experiment to verify that a single product per primer pair was amplified. Threshold cycle values were used to calculate the fold change in the transcript levels by using the $2-\Delta\Delta Ct$ method. The relative miRNA expression levels were normalized to the *GAPDH* gene. Each qRT-PCR group had 3 or 4 biological replications.

Immunohistochemistry

Mice were euthanized by intraperitoneal injection of an overdose concentration of chloral hydrate, and were transcardially perfused with 100 mL saline (0.9% w/v NaCl), followed 4% paraformaldehyde (PFA). The brain was removed and post-fixed in 4% PFA, and then 30 μm sagittal or coronal sections were cut (Leica Microsystems, Wetzlar, Germany).

Immunohistochemistry was applied to free-floating brain sections as described previously [34–36]. In brief, 30-μm free-floating sections of the hippocampus were stained and blocked in 3% normal goat serum at room temperature for 1 h. Then the sections were incubated overnight with one of the following primary antibodies: mouse-anti-eIF4E (Proteintech Group, Cat#66655-1-lg), rabbit-anti-Iba1 (Wako, 1: 1000, Cat#019-19741), mouse-anti-GFAP (Cell Signaling Technology, 1:1000, Cat#3670), or rabbit-anti-NeuN (Abcam, 1:500, Cat#ab177487). Then they were washed with PBS and reacted with conjugate-adsorbed Alexa Fluor 488 donkey anti-mouse, Alexa Fluor 488 donkey anti-rabbit, Alexa Fluor 546 donkey anti-mouse, and Alexa Fluor 546 donkey anti-rabbit for 60–90 min. To label the nucleus, cells were also incubated with DAPI (Invitrogen, 1:1500, Cat#62248) for 5 min. The sections were rinsed, dried, and coverslipped with fluorescence mounting medium. Control sections were processed with omission of the primary antisera. A laser-scanning confocal microscope (LSM 800; Zeiss) was used for fluorescence imaging.

Luciferase Reporter Assay

Human embryonic kidney 293 cells were co-transfected with miR-34b-3p mimics or a scrambled control and wild-type or mutant eIF4E 3'-UTR plasmids. Cells were harvested and lysates were used for firefly and *Renilla* luciferase activity using a dual-luciferase reporter assay kit (Promega, E1910) according to the manufacturer's protocol. The normalized values (*Renilla*/firefly activity) were used for analysis. Each group had three biological replications. The miR-34b-3p mimics/antagomirs and the scrambled control were from RioBio (Guangzhou, China). The miR-34b-3p overexpression construct was from GeneCopoeia (Rockville, MD). The 3′-UTR of eIF4E was amplified with the following primers: forward 5′-GGACTTTGCTGGTGTGAGAGT-3′, reverse 5′-CCTGGATCCTTCACCAATGTT-3′. The polymerase chain reaction fragment was inserted into psiCHECK2 (Promega, Madison, WI) within the XhoI and NotI restriction sites. Mutations were generated using a fast mutation kit from Agilent (Brighton, MA).

Western Blot

Hippocampi isolated from the mice were homogenized in ice-cold lysis buffer containing 50 mmol/L Tris-HCl, pH 8.0, 150 mmol/L NaCl, 1% NP-40, 0.5% sodium deoxycholate, 0.1% SDS, 0.02% NaN_3, 100 mg/mL PMSF, and 10 mg/mL each of the protease inhibitors (Thermo Scientific, 1 mL/10 g tissue) and collected the homogenate to centrifuge at 12,000 g at 4°C for 5 min; aliquots of supernatants were added to one-third volume of 4× sample buffer, followed by boiling for 10 min and then sonication for 5 s on ice. Protein concentration was quantitated using the BCA Protein Assay Reagent (Pierce). The protein samples were separated on 12% SDS-PAGE gels. Proteins were transferred to nitrocellulose filter membranes (NC) using a Bio-Rad Miniprotein III System wet transfer unit. After incubation with blocking solution (5% nonfat dried milk) for 30 min at room temperature, the transfer membranes were incubated with primary antibody diluted with 3% bovine serum albumin in TBST buffer overnight at 4°C. The membranes were incubated with secondary antibodies for 1 h at room temperature on the next day. Signals were detected with an infrared imaging system (Odyssey, Li-Cor).

Stereotaxic Injection

Mice (C57BL/6 males, 6 weeks old for electrophysiological experiments, 10 weeks old for behavioral and protein qualification experiments) were anesthetized with 5% chloral hydrate and placed in a stereotaxic apparatus. The head was fixed and the skull was exposed. Burr holes were made and a micro syringe (World Precision Instruments) was slowly lowered into the following injection site: AP, –2.18 mm; ML, –1.38 mm; DV, –1.60 mm from bregma. 1 μL of virus was pressure-injected into each hippocampus at 0.1 μL/min (total volume 1 μL). Before suture, the needle remained in place for 5 min and was then slowly retracted to avoid leakage. Then the mice were left on a heating pad throughout recovery from anesthesia. Electrophysiological and behavioral experiments were started 4 weeks after the virus injection. Adeno-associated viruses (AAVs) for eIF4E overexpression and eIF4E siRNA were from Genechem (Shanghai, China) and Taitool Bioscience (Shanghai, China), respectively.

Electrophysiological Recordings

Hippocampal slices (300 μm) were prepared as previously described [35]. The slices were then transferred to a holding chamber containing artificial cerebrospinal fluid (ACSF, in mmol/L: 124 NaCl, 3 KCl, 26 $NaHCO_3$, 1.2 $MgCl_2$, 1.25 $NaH_2PO_4{\cdot}2H_2O$, 10 glucose, and 2 $CaCl_2$ at pH 7.4, 305 mOsm) at 32°C for 30 min. After 60 min of recovery at room temperature, slices were transferred to a recording chamber, which was continuously perfused with 95% O_2 /5% CO_2-saturated ACSF (2 mL/min) at room temperature. For excitability analysis, the action potential was recorded with an internal solution containing (in mmol/L) 140 potassium gluconate, 10 HEPES, 0.2 EGTA, 2 Mg^{2+}ATP, 2 NaCl, and 0.3 NaGTP, adjusted to pH 7.4 with KOH, 290–295 mOsm. We made whole-cell current-clamp recordings from $eIF4E^+$ and $eIF4E^-$ granule neurons, which were visualized under a fluorescent infrared phase-contrast Axioskop 2FS upright microscope equipped with a Hamamatsu C2400-07E

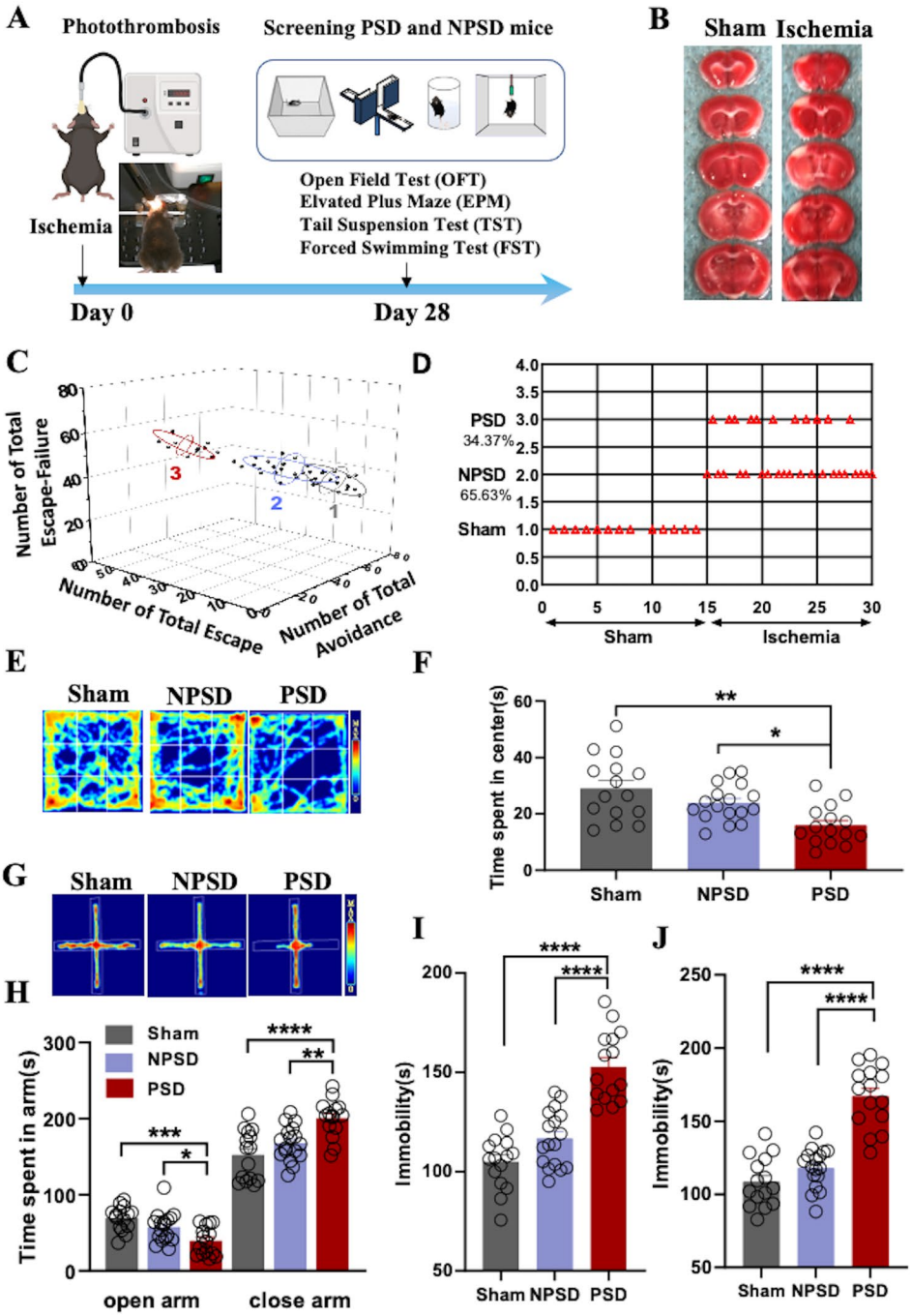

infrared camera. The raw electrophysiological data were collected at 10 kHz and filtered with a low-pass filter at 2 kHz and analyzed using Clampfit 10.2 software (Molecular Devices). Input resistance and access resistance were monitored continuously throughout each experiment; experiments were terminated if these changed by >20%.

Reagents and Antibodies

The following antibodies and chemicals were used: anti-eIF4E (Proteintech Group 66655-1-lg); anti-PRKAR2B (Abcam ab75993); anti-Gpm6a (ABclonal A9066); anti-Ntng1 (ABclonal A17875); anti-β-actin (Proteintech Group, 66009-1-lg); anti-Iba1 (Wako, 019-19741); anti-GFAP (Cell Signaling Technology, 3670); anti-NeuN (Abcam, ab177487); rose Bengal (Sigma-Aldrich 632-69-9); TTC (Sigma-Aldrich, 298-96-14).

◂**Fig. 1** Screening and identification of mice with a post-stroke depression-like phenotype **A** Schematic of the timeline and protocol of this study. **B** Representative TTC-stained images taken 24 h after operation. **C** A three-dimensional spatial scatterplot showing 3 types of cluster based on the total number of escapes, total number of escape-failures, and total number of avoidances. Data with similar characteristics are linked together by lines and form a cluster. In each cluster, the standard error of each type is represented by ellipses. Cluster 1 represents the sham mice; cluster 2 corresponds to the ischemic mice without depression, namely non-post-stroke depression (NPSD) mice; and Cluster 3 is related to ischemic mice with very high levels of depression, namely post-stroke depression (PSD) mice. **D** The unsupervised fuzzy clustering method was used for cluster analysis of behavioral data to obtain partitioned clusters of all mice with hard categories. The red "Δ" attached to a specific coordinate indicates the corresponding cluster number of the tested mouse. **E** Representative images showing the OFTs of sham, NPSD, and PSD mice. **F** OFT bar graph showing the time spent in the center by sham, NPSD, and PSD groups. Data are the mean ± SEM ($n=15$ in sham and NPSD groups, $n=17$ in PSD group; sham *vs* PSD $^{**}P=0.0024$, NPSD *vs* PSD $^{*}P=0.0103$, $F=8.653$, one-way ANOVA followed by Bonferroni multiple comparisons). **G** Representative images showing the EPM test of sham, NPSD and PSD mice. **H** EPM bar graph showing the time spent in open arms (left) and closed arms (right) of sham, NPSD, and PSD mice. Data are the mean ± SEM ($n=15$ in sham and NPSD groups, $n=17$ in PSD group; in open arm, sham *vs* PSD $^{***}P=0.0001$, NPSD *vs* PSD $^{*}P=0.0195$, $F=10.45$, in closed arm, sham *vs* PSD $^{****}P<0.0001$, NPSD *vs* PSD $^{**}P=0.0033$, $F=12.98$, one-way ANOVA followed by Bonferroni multiple comparisons). **I**, **J** Immobility time as an indicator of depression-like behaviors in TST (**I**) and FST (**J**) in sham ($n=15$), NPSD ($n=17$) and PSD ($n=15$) mice, in TST, sham *vs* PSD $^{****}P<0.0001$, NPSD *vs* PSD $^{****}P<0.0001$, $F=40.52$, in FST, sham *vs* PSD $^{****}P<0.0001$, NPSD *vs* PSD $^{****}P<0.0001$, $F=49.97$. OFT, open field test; EPM, elevated plus maze test; TST, tail suspension test; FST, forced swim test.

Statistical Analysis

Statistical analyses were performed using GraphPad Prism 8.0. All data are represented as the mean ± SEM. Statistically significant differences were defined as ns, not significant, $^{*}P<0.05$, $^{**}P<0.01$, $^{***}P<0.001$, $^{****}P<0.0001$, unpaired two-tailed Student's *t* tests were used in Western blots, and repeated one-way ANOVA and *post hoc* Bonferroni corrections following two-way analyses of variance (BF ANOVA) in all behavioral when assumptions of normality and equal variance (*F* test) were met.

Results

Screening and Identification of Mice with a Post-stroke Depression-like Phenotype

We established the mouse model of local cortical ischemia induced by photothrombosis based on our previous studies [30]. After intravenous injection of rose Bengal into mice, the cortical region was illuminated with a 150 W cold light to induce cortical vascular thrombosis, which led to ischemic injury in the cortex (Fig. 1A). TTC staining was used to confirm ischemic lesions in the cortical area. We found that the ischemic mice had distinct unstained cortical areas in the side ipsilateral to the illumination compared with the contralateral side or the brain of sham control mice. This result demonstrated successful photothrombosis-induced local cortical ischemia. (Fig. 1B).

To screen the post-stroke depression-like phenotype from both ischemic and sham mice, we applied unsupervised fuzzy clustering to analyze all the behavioral parameters collected from 45 mice (Fig. S1). The results showed that the full range of the data set was classified into three clusters (Fig. 1C). Cluster 1 partially overlapped with cluster 2, while cluster 3 was clearly separated from clusters 1 and 2. Cluster 3 corresponded to the ischemic mice and was characterized by higher levels of depression, namely PSD mice. Cluster 2 corresponded to the ischemic mice and was characterized by very low levels of depression or a non-depressed state, namely NPSD mice. Cluster 1 described the sham-operated mice associated with a non-depressed state, namely Sham mice (Fig. 1D). Further analysis of the behavioral results revealed that 34.37% of the ischemic population was associated with cluster 3 (PSD), whereas 65.63% from among the ischemic mice was associated with cluster 2 (ischemia without depression-like symptoms, NPSD). In the sham-control group, all 13 mice were associated with Cluster 1 (Sham).

Then, we used the OFT, the EPM, the TST, and the FST to verify the PSD-like behavioral phenotype. The OFT results confirmed that the screened PSD mice displayed a substantially decreased time spent in the center area when compared with Sham or NPSD mice (Fig. 1E, F). The EPM data also confirmed that the screened PSD mice spent a significantly shorter time in the open arm and a robustly longer duration in the closed arm than the sham or NPSD mice (Fig. 1G, H). However, there was no significant difference in the distance and speed of movement among PSD, NPSD, and sham mice in the OFT and EPM experiments (Fig. S2). Moreover, both the TST and the FST showed that the immobility time was significantly prolonged in the screened PSD mice compared to the sham or NPSD mice (Fig. 1I, J). The above results suggest that the mouse model of cerebral ischemic stroke induced by light thrombosis can be screened and the PSD and NPSD phenotypes can be distinguished through multiple behavioral tests and unsupervised fuzzy clustering algorithms. And the screened PSD and NPSD mice can be further confirmed by depression-like behavioral experiments. The percentage of PSD mice is consistent with the epidemiological profile of depressed patients after cerebral ischemic stroke.

The Hippocampus of PSD Mice Exhibits Secondary Degeneration

Measurement of 18-fluoro-6-deoxy-glucose (FDG) in the brain by positron emission tomography (PET) reflects the level of glucose metabolism in the brain, which in turn indicates the degree of neural activity [37]. Therefore, we applied PET scan imaging to the mouse brain (Fig. 2A) to define which brain regions are involved in the occurrence of PSD after focal cortical ischemia. The brain images of FDG-PET scanning showed that the level of glucose metabolism in some brain regions of PSD mice was clearly weaker than that of the Sham control group (Fig. 2B). Statistical analysis on the mean standardized uptake value (SUV) of FDG showed that, compared with Sham or NPSD mice, the mean SUVs in the lateral striatum, cortex, hippocampus, thalamus, and basal forebrain septum were significantly reduced in PSD mice. In particular, the reduction in the hippocampus was the most significant. However, no significant change was found in the other brain regions between sham, NPSD, and PSD mice (Fig. 2C, D). Subsequently, to confirm the FDG-PET imaging results, we used FJ staining to demonstrate the degenerative alterations in the mouse brain sections. The FJ staining results confirmed an apparent increase in the number of FJ^+ cells in the hippocampal region of PSD mice as compared with sham and NPSD mice (Fig. 2E, F). The

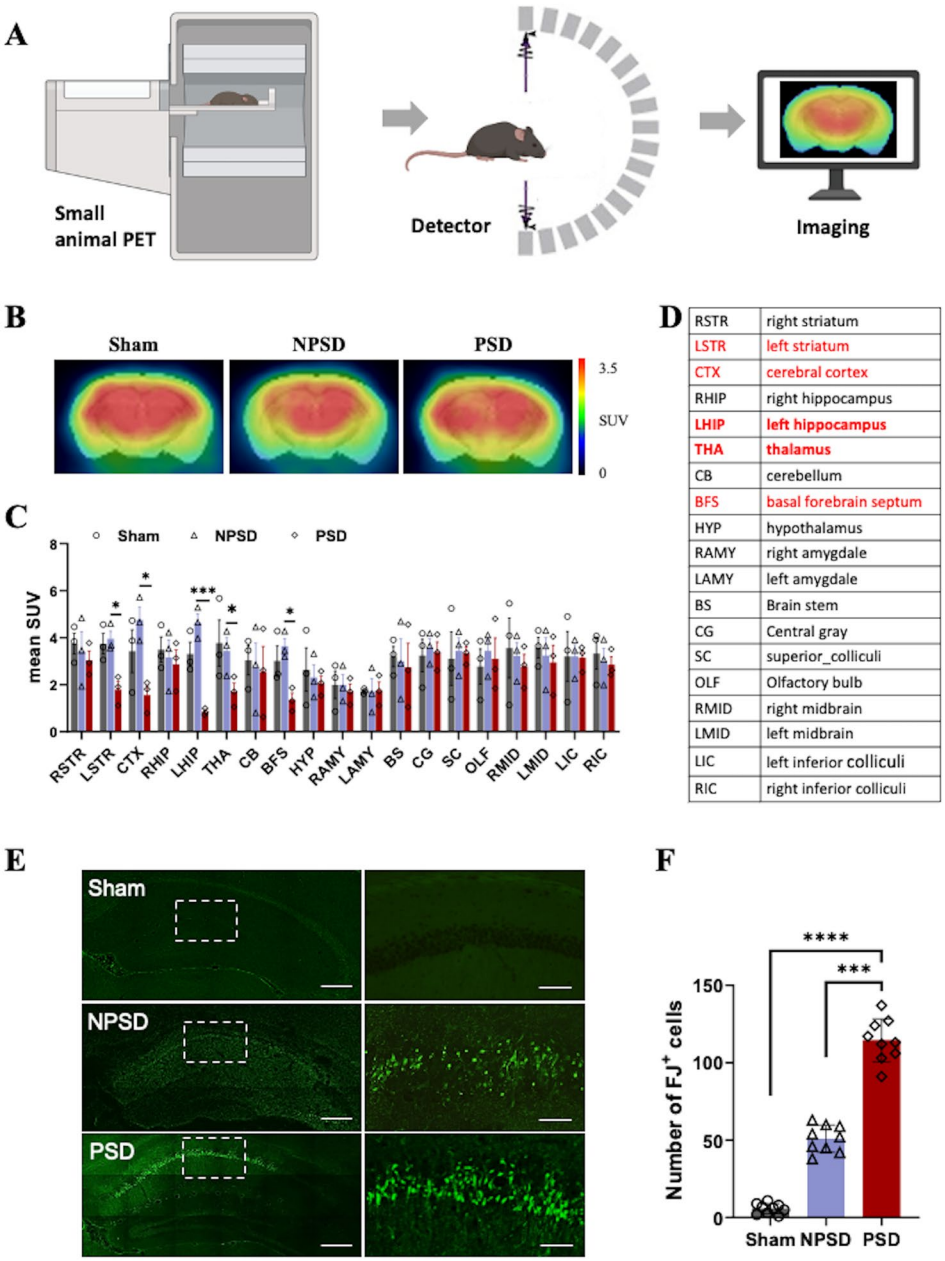

Fig. 2 PSD mice exhibit secondary degeneration in the hippocampus **A** Schematic of the process of PET imaging of mouse brain. **B** Representative images of PET scans of coronal sections of mouse brain in Sham control, NPSD, and PSD groups. **C** Statistics of the standard uptake value (SUV) of PET scan images showing glucose metabolism in the lateral striatum (*$P=0.0202$, $F=9.981$), cortex (*$P=0.0443$, $F=5.786$), left hippocampus (***$P=0.001$, $F=27.8$), thalamus (*$P=0.0226$, $F=8.883$), and basal forebrain septum (*$P=0.032$, $F=7.131$) is significantly reduced compared with the NPSD group, while other brain regions show no significant changes. Data are the mean ± SEM ($n=6$ per group). **D** List of abbreviations and full names of the brain regions examined; those with significant changes are in red. **E** Representative images of Fluoro Jade (FJ) staining of coronal sections showing a significant increase in FJ-positive (FJ^+) neurons in hippocampal regions of the PSD group compared with the NPSD group [scale bars, 20 μm (left), 100 μm (right)]. **F** statistical histogram of the number of FJ^+ neurons. Data are mean ± SEM ($n=6$ in each group, sham *vs* PSD ****$P < 0.0001$, PSD *vs* NPSD ****$P < 0.0001$, $F=289.4$).

above results demonstrated that PSD mice with localized primary ischemia in the cortex have significant secondary degenerative changes in the hippocampus.

miR34b-3p Is Downregulated in the Hippocampus of PSD Mice

To reveal the specific molecules in the hippocampus involved in PSD, we acutely isolated hippocampal tissue from Sham, NPSD, and PSD mice for RNA-seq analysis (Fig. 3A). Volcano plots for group-to-group comparisons of miRNAs from Sham, NPSD, and PSD mice showed that 64 miRNAs were up-regulated and 22 were down-regulated in PSD compared with the Sham group (Fig. 3B), 19 were up-regulated and 20 were down-regulated in PSD compared with the NPSD group (Fig. 3C), and 31 were up-regulated and 16 were downregulated in Sham compared with the NPSD group (Fig. 3D). Next, to further clarify the specific miRNAs involved in PSD, we intersected the up- and down-regulated miRNAs derived from group-to-group

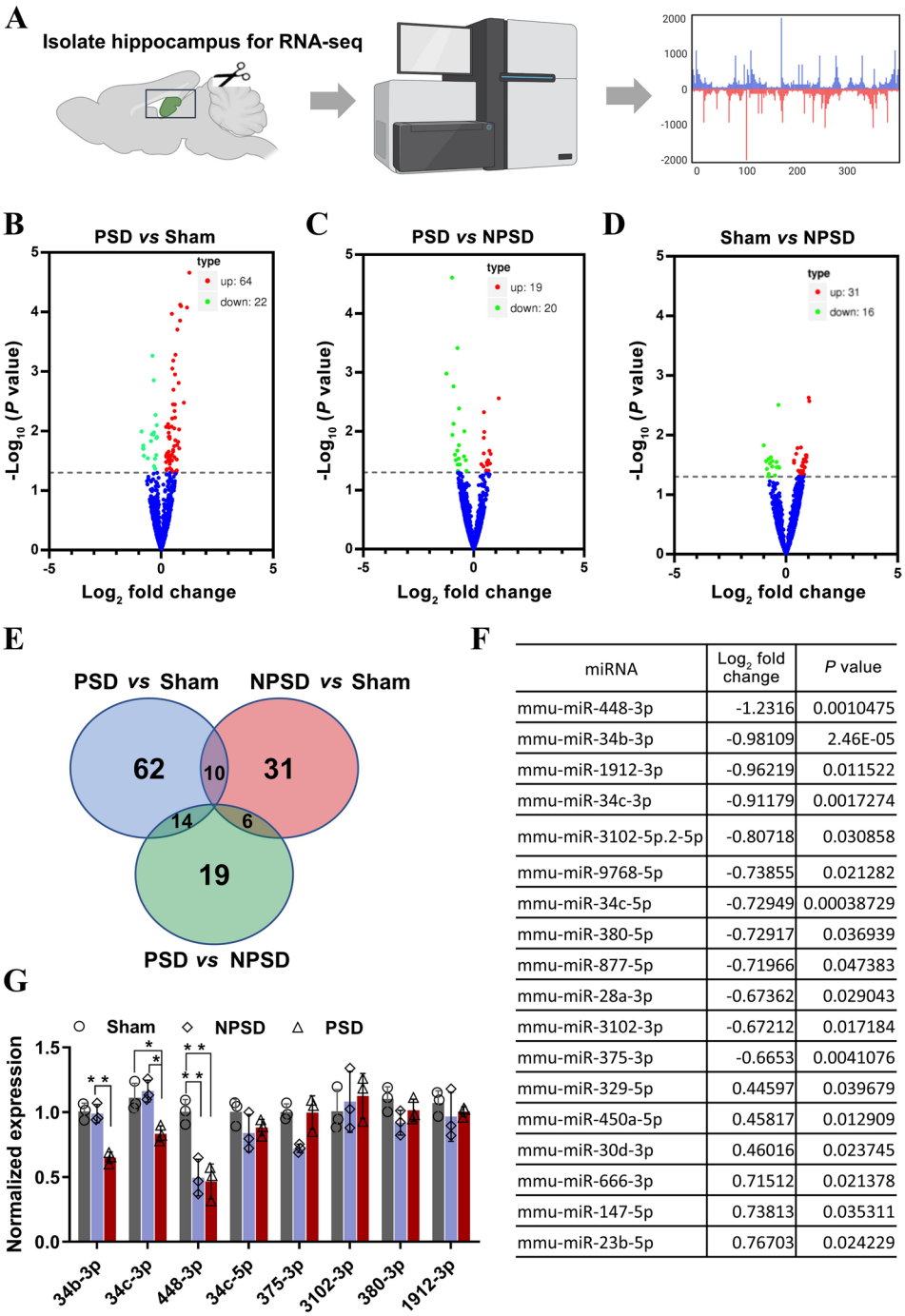

F

miRNA	Log_2 fold change	*P* value
mmu-miR-448-3p	-1.2316	0.0010475
mmu-miR-34b-3p	-0.98109	2.46E-05
mmu-miR-1912-3p	-0.96219	0.011522
mmu-miR-34c-3p	-0.91179	0.0017274
mmu-miR-3102-5p.2-5p	-0.80718	0.030858
mmu-miR-9768-5p	-0.73855	0.021282
mmu-miR-34c-5p	-0.72949	0.00038729
mmu-miR-380-5p	-0.72917	0.036939
mmu-miR-877-5p	-0.71966	0.047383
mmu-miR-28a-3p	-0.67362	0.029043
mmu-miR-3102-3p	-0.67212	0.017184
mmu-miR-375-3p	-0.6653	0.0041076
mmu-miR-329-5p	0.44597	0.039679
mmu-miR-450a-5p	0.45817	0.012909
mmu-miR-30d-3p	0.46016	0.023745
mmu-miR-666-3p	0.71512	0.021378
mmu-miR-147-5p	0.73813	0.035311
mmu-miR-23b-5p	0.76703	0.024229

Fig. 3 miR34b-3p is down-regulated in the hippocampus of PSD mice **A** Schematic of the protocol of RNA-sequencing. **B–D** Volcano plots of differentially-expressed miRNA between PSD and sham (**B**), PSD and NPSD (**C**), and sham and NPSD (**D**). The plots show a log_2 fold change in expression between the groups on the x-axis and the negative log_{10} *P* values on the y-axis. Red, significantly up-regulated; green, significantly down-regulated; blue no significant difference with FDR <0.05. **E** Venn diagram of differentially-expressed miRNAs. **F** Table summarizing the differentially-expressed miRNAs between PSD and NPSD, excluding those repeated in PSD *vs* sham and sham *vs* NPSD **G** Validation of some of the down-regulated miRNAs in Table **F** by qRT-PCR (in 34b-3p, NPSD *vs* PSD $^{**}P=0.0014$, $F=33.25$, in 34c-3p, NPSD *vs* PSD $^{*}P=0.0164$, sham *vs* PSD $^{*}P=0.0354$, $F=10.38$ in 448-3p, sham *vs* NPSD $^{**}P=0.0077$, NPSD *vs* PSD $^{**}P=0.0058$, $F=17.35$).

comparisons and plotted a Wayne diagram (Fig. 3E), which showed 19 differentially expressed miRNAs in the PSD *versus* NPSD groups (Fig. 3F). Validation of the above miRNAs by qPCR revealed that miR34b-3p, miR34c-3p, and miR448-3p were dramatically down-regulated in the hippocampus of PSD mice. Among them, only the expression of miR-34b-3p did not change significantly in the NPSD and Sham groups (Fig. 3G). These results suggest that the decreased expression of miR34b-3p in the hippocampus may be specifically associated with the development of PSD.

NPSD Mice Show PSD-like Changes After Downregulation of miR-34b-3p in the Hippocampus

To further confirm that miR-34b-3p in the hippocampus is involved in the development of PSD, we injected an antagonist of miR-34b-3p (A-miR-34b) into the hippocampus of the screened NPSD mice and observed the behavioral changes before and after injection (Fig. 4A). HE staining of coronal sections of the mouse brain showed the correct injection site in the hippocampus (Fig. 4B). The qPCR results showed that A-miR-34b downregulated the expression level

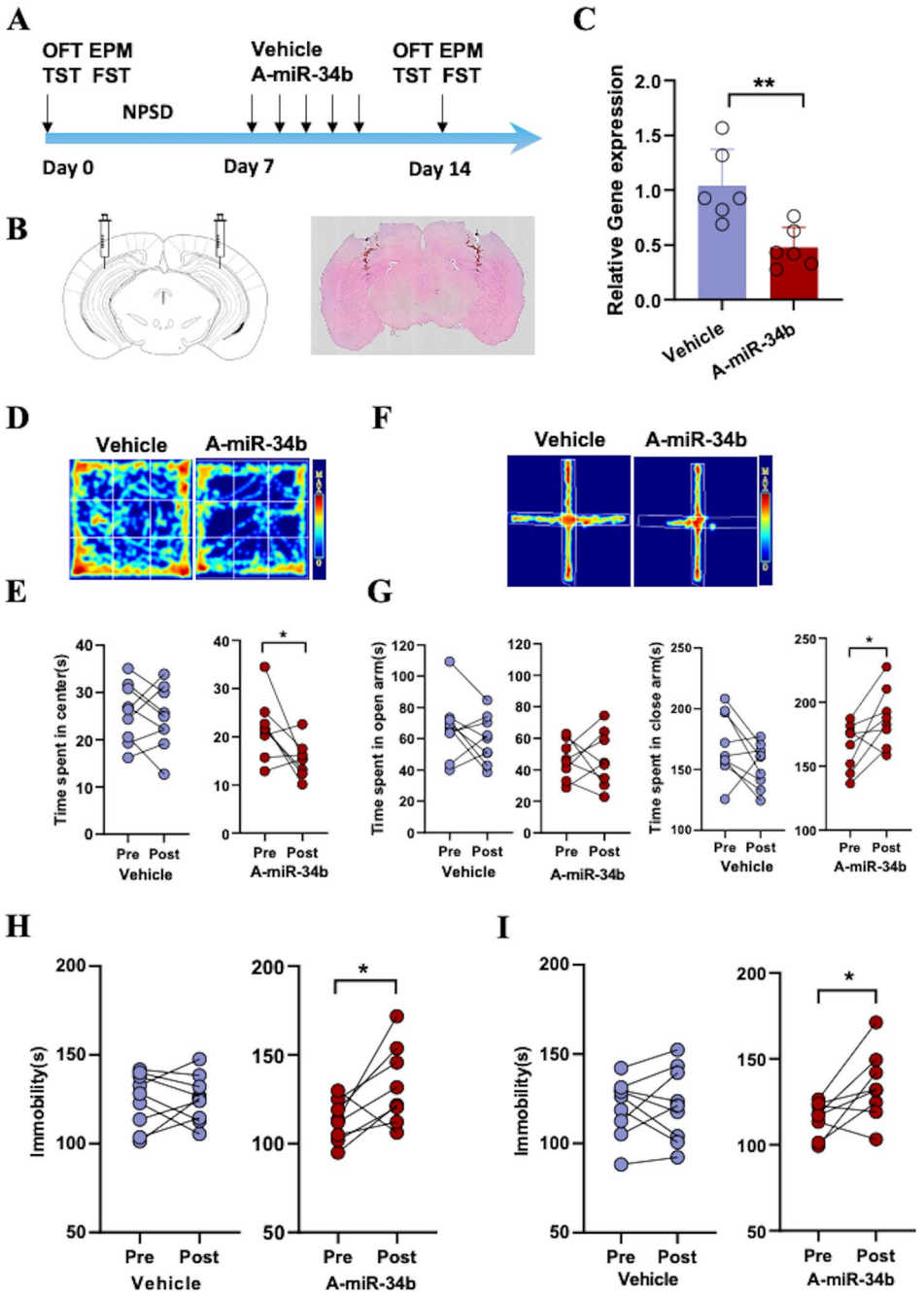

Fig. 4 NPSD mice show PSD-like changes after downregulation of miR-34b-3p in the hippocampus **A** Schematic of the timeline and protocol of this study. **B** Representative images of a hematoxylin-stained coronal brain section at the injection sites. **C** Relative miRNA-34b-3p expression in the hippocampus of the vehicle group and the antagomir miRNA-34b-3p(A-miR-34b) group. Data are the mean ± SEM ($n=6$ per group, $^{**}P=0.0046$) **D–I** Behaviors of mice injected with Vehicle or antagomirs of miRNA-34b-3p(A-miR-34b). **E** Time spent in the center by NPSD mice before and after applying vehicle ($n=9$) or A-miR-34b ($n=8$), $^{*}P=0.0286$. **G** Time spent in open arms (left) and closed arms (right) by NPSD mice before and after applying vehicle ($n=9$) or A-miR-34b ($n=8$), $^{*}P=0.0468$. **H** Immobility time in TST of NPSD mice before and after applying vehicle ($n=9$) or A-miR-34b ($n=8$), $^{*}P=0.0403$. **I** Immobility time in FST of NPSD mice before and after applying vehicle ($n=9$) or A-miR-34b ($n=8$), $^{*}P=0.0351$.

of miR-34b-3p 50%~1-fold compared to the Vehicle control (Fig. 4C). These results indicate that A-miR-34b was successfully injected into the hippocampal region and was able to exert antagonistic effects against miR-34b-3p.

Next, we examined the effect of A-miR-34b on the behaviors of NPSD mice. The OFT results showed that NPSD mice injected with A-miR-34b-3p spent markedly less time in the central zone than before injection. And there was no significant change before and after Vehicle injection (Fig. 4D, E). The EPM data also showed that NPSD mice injected with A-miR-34b spent a remarkably shorter time in the open arm and notably longer duration in the closed arm, while these parameters did not change before and after Vehicle injection (Fig. 4F, G). In addition, the results of both TST and FST revealed that NPSD mice spent more time immobile after A-miR-34b injection than before injection. As expected, no significant change on the immobility time was observed in NPSD mice pre- and post-Vehicle injection (Fig. 4H, I). Taken together, these results suggest that downregulation of miR-34b-3p in the hippocampus of NPSD mice induces PSD-like behavior.

eIF4E Is a Target Gene of miR-34b-3p

MiRNAs are known to bind to the untranslated region at the 3′ end (3′-UTR) of the target mRNA and promote mRNA degradation or inhibit mRNA translation, further affecting the expression of the target gene. Therefore, to find the target gene of miR-34b-3p, we first predicted its target genes by applying the most commonly-used miRNA prediction softwares: TargetScan, miWalk, and miRDB. Each of these programs predicted a large number of possible target genes. By intersecting the predictions, the number of predicted genes was reduced to 196 (Fig. 5A). Subsequently, we performed GO enrichment analysis for the predicted target genes, and 42 genes were closely associated with neurobiological functions, such as synaptic transmission, axonal fasciculation, neuron migration, RNA splicing, and nervous system development (Figs 5B, S3). We then applied comprehensive tools, mirSVR Score, Target Score and Cumulative weighted context score, for sequence-based miRNA target prediction to further score the above 42 target genes. Among them, *eIF4E, Gpm6a, Ntng1, and Prkar2b*, had significantly higher scores than other genes (Fig. 5C). We next confirmed that these 4 genes encoded proteins by western blot. We found that only the eIF4E protein level was robustly increased in the hippocampal tissue of PSD mice, compared with NPSD or Sham mice. While the protein levels of Gpm6a, Ntng1, and Prkar2b showed no significant changes among the three groups (Fig. 5D, E). Through sequence alignment, we found that the 3'UTR sequence of *eIF4E* is highly conserved across species. Based on this, we designed mutated *eIF4E* (Mut) by disrupting the 3'UTR sequence, and used wild-type *eIF4E* (WT) with the normal 3'UTR sequence as a control, to further confirm *eIF4E* as a target gene of miR-34b-3p (Fig. 5F). Based on the sequence of miR-34b-3p, we also synthesized its analog (Mimic) and the disrupted sequence (Scrambled) as a control. Luciferase reporter experiments showed that Mimic, but not Scrambled, of miR-34b-3p dramatically down-regulated the WT of *eIF4E*. Neither Mimic nor Scrambled of miR-34b-3p had a significant downregulation effect on the Mut of *eIF4E* (Fig. 5G). The above results indicate that *eIF4E* is indeed a target gene of miR34b-3p. To detect the cellular localization of eIF4E and miR-34b-3p in the hippocampus, we used *in situ* hybridization with double immunofluorescent labelling and observed that miR-34b-3p was localized in neurons, but not microglia and astrocytes. Meanwhile, both *eIF4E* and miR-34b-3p were co-expressed in neurons of the hippocampus (Fig. 5H, S4). This result suggests that miR-34b-3p may participate in the development of PSD by targeting *eIF4E* in hippocampal neurons.

Downregulation of eIF4E in Hippocampal Neurons Improves Depression-Like Behavior in PSD Mice

To further explore the therapeutic strategy for PSD, we constructed AAV2/9-si-eIF4E-eGFP (Si-eIF4E) for downregulation of eIF4E by using a lentivirus vector carrying small interfering RNA. And AAV2/9-scrambled-eIF4E-eGFP (Scr-eGFP) was designed as a control (Fig. 6A). The detailed plasmid information with target sequences and primer sequences for eIF4E are available in the Supplementary Material (Fig. S5). We first injected AAV into the hippocampal region of PSD mice screened in the ischemia model and performed behavioral assays three weeks later. The mice were sacrificed at the end of the behavioral tests to confirm the expression of AAV in the hippocampal region (Fig. 6B). Three weeks after infection with AAVs, hippocampal pyramidal cells in brain sections from NPSD mice showed abundant green fluorescence, with typical neuronal cell bodies and fibers (Fig. 6C). In addition, we performed western blot experiments on hippocampal tissues infected with AAV virus, and the results showed that the protein band density of eIF4E was significantly reduced in the Si-eIF4E group compared to the Scr-eIF4E group (Fig. 6D, E). The above results showed that our AAV-Si-eIF4E successfully infected the hippocampal neurons of PSD mice and downregulated the expression of eIF4E. The behavioral results showed that, compared to the pre-injection group, there was a tendency to increase the time in the central area of the OFT in PSD mice after Si-eIF4E injection (Fig. 6F), and the time in the open arm was significantly longer in the EPM test (Fig. 6G). In addition, the immobility time of PSD mice after Si-eIF4E injection was significantly shorter in both the TST (Fig. 6H) and the FST (Fig. 6I). However, there were no significant changes in the above behavioral parameters

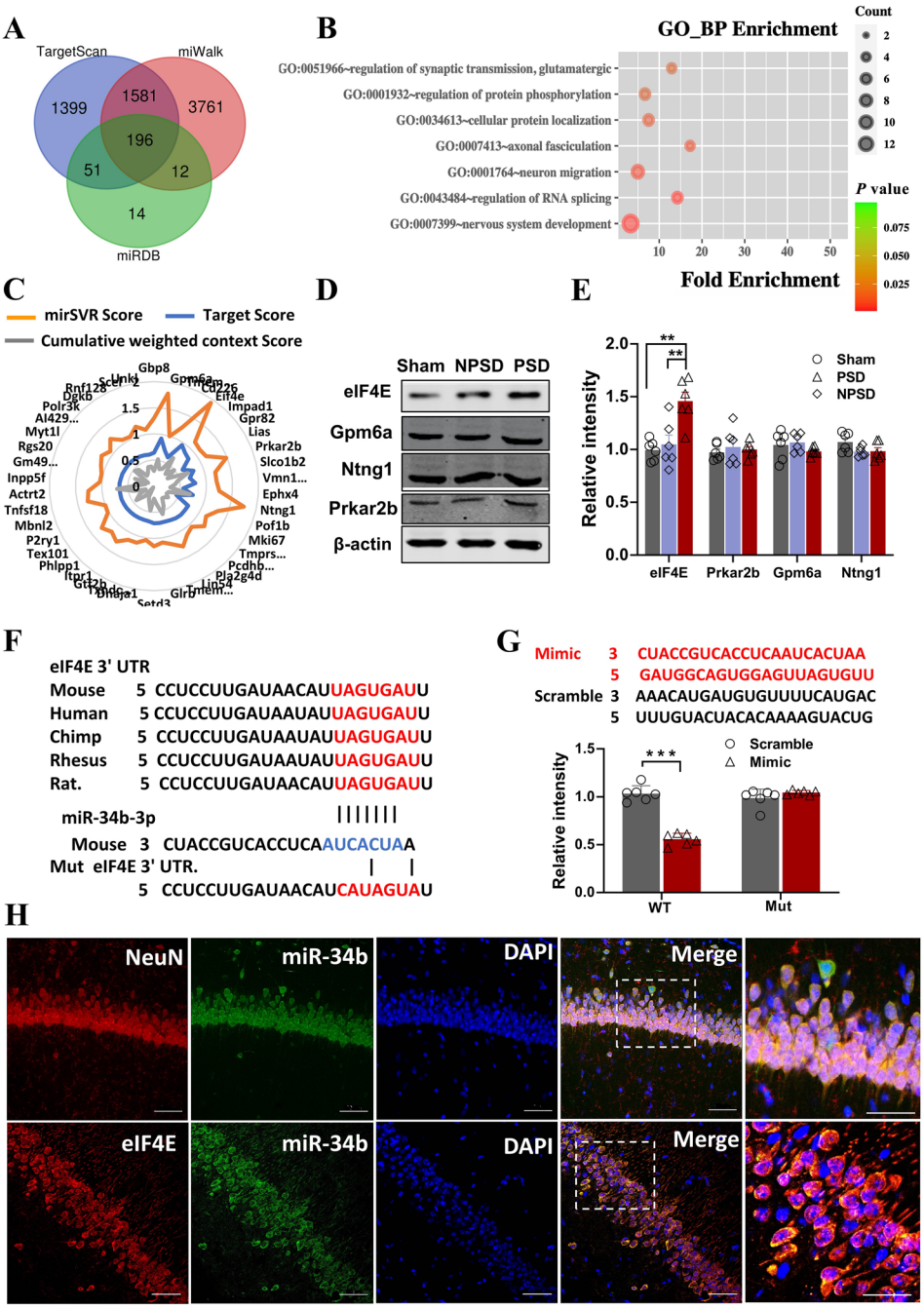

Fig. 5 *eIF4E* is a target gene of miR-34b-3p **A** Venn diagram of miRNA-34b-3p silico prediction co-applied with TargetScan, miWalk, and miRDB. **B** Predicted target genes for the GO biological process (BP) function enrichment. An example comparison of the top 7 pathways; the size of the point represents the proportion of the number of genes enriched in a given pathway in the background, the colors of the dots represents p values, while the red-to-green gradient shows the statistical significance from strong to weak. **C** Radar map showing the results of mirSVR Score, Target Score, and Cumulative weighted context score on the 42 sequence-based miRNA-34b-3p target genes. **D, E** Representative western blots (**D**) of cell lysates from the hippocampus of sham, NPSD, and PSD mice and bar graph (**E**) showing the band intensities normalized to the respective controls (defined as 1.0). Data are the mean ± SEM ($n=6$ per group; in eIF4E group, sham *vs* PSD $^{**}P=0.0016$, NPSD *vs* PSD $^{**}P=0.0045$, $F=11.5$). **F** Sequence analysis showing that the miR-34b-3p binding region in the *eIF4E* 3′UTR is conserved in mammals. The mutant sequence in 3′UTR of *eIF4E* for luciferase analysis is shown below. **G** The wild-type (WT) or mutant (Mut) 3′UTR of *eIF4E* in the psiCHECK-2 vector was co-transfected into HEK293T cells with miR-34b-3p mimics (Mimic) or scrambled control (Scramble). The luciferase activity was determined at 48 h after the transfection ($n=6$ per group, $^{***}P=0.0001$). The sequences of Mimic and Scramble are shown above. **H** Representative confocal images of co-immunofluorescence staining with miR-34b-3p probe (green) and the antibody of NeuN (red, upper) and eIF4E (red, lower) in the hippocampus of mice (scale bars, 50 μm).

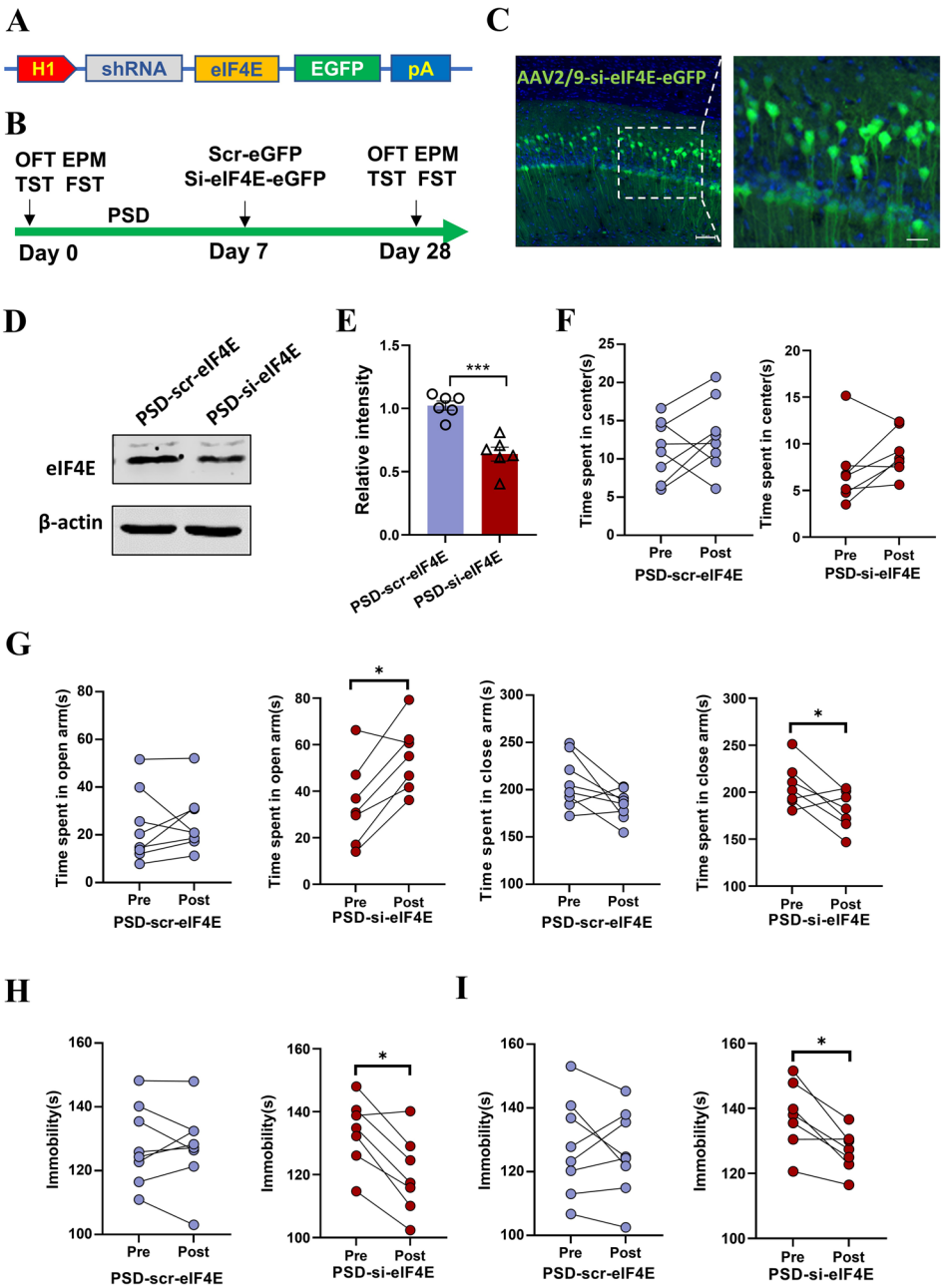

Fig. 6 Downregulation of eIF4E in hippocampal neurons improves depression-like symptoms in PSD mice **A** Diagram of the AAV construct for silencing eIF4E. **B** Schematic of the timeline and protocol of this study. **C** Representative fluorescence images of a virus-infected slice [scale bars, 50 μm (left), 20 μm (right)]. **D** Representative band images of western blots of cell lysates from the hippocampus showing the eIF4E expression of PSD-scr-eIF4E mice and PSD-si-eIF4E mice **E** Bar graph showing the band intensities normalized to β-actin. Data are the mean ± SEM ($n=6$ per group, $^{***}P=0.0002$). **F–I** Behavioral tests of PSD mice injected with AAV-scr-eIF4E or AAV-si-eIF4E. **F** Center time in the OFT of PSD mice before and after applied AAV-scr-eIF4E ($n=8$) or AAV-si-eIF4E ($n=7$). **G** Time spent in open arms (left) and closed arms (right) of the EPM by PSD mice before and after applied AAV-scr-eIF4E ($n=8$) or AAV-si-eIF4E ($n=7$), $^{*}P=0.0409$ (left), $^{*}P=0.0488$ (right). **H** Immobility time in the TST of PSD mice before and after applied AAV-scr-eIF4E ($n=8$) or AAV-si-eIF4E ($n=7$), $^{*}P=0.0493$. **I** Immobility time in the FST of PSD mice before and after applied AAV-scr-eIF4E ($n=8$) or AAV-si-eIF4E ($n=7$), $^{*}P=0.0389$.

before and after Scr-eIF4E injection. The above behavioral results suggest that downregulation of eIF4E in hippocampal neurons does improve depression-like behavior in PSD mice.

Overexpression of eIF4E in Hippocampal Neurons of NPSD Mice Induces Depression-like Behavior

To confirm the role of eIF4E in the development of PSD, we constructed AAV2/9-eIF4E-eGFP (eIF4E) for overexpression of eIF4E by using a lentivirus vector carrying eIF4E. And AAV2/9-eGFP (eGFP) was designed as a control (Fig. S6A). We first injected AAV into the hippocampal region of NPSD mice and performed behavioral assays three weeks later (Fig. S6B). The mice were sacrificed at the end of the behavioral tests to verify the expression of AAV in the hippocampal region. Three weeks after infection with AAVs, hippocampal pyramidal cells in brain sections from NPSD mice showed abundant green fluorescence, with typical neuronal cell bodies and fibers (Fig. S6C). In addition, we performed western blot experiments on hippocampal tissue infected with AAV, and the results showed that the protein band density of eIF4E was significantly higher in the eIF4E group than in the eGFP group (Fig. S6D). The above results showed that eIF4E was successfully overexpressed in the

hippocampal neurons of NPSD mice. The behavioral results showed that, compared to the pre-injection group, there was a tendency to decrease the time in the central area of the open field in NPSD mice after eIF4E injection (Fig. S6E), and the time in the open arm was significantly shortened (Fig. S6F) in the EPM test, while the time in the closed arm was significantly prolonged (Fig. S6G). In addition, the immobility time of PSD mice after eIF4E injection was significantly increased in both the TST (Fig. S6H) and the FST (Fig. S6I). However, there were no significant changes in the above behavioral parameters before and after eGFP injection. To test whether overexpression of eIF4E has an effect on neuronal function, we made patch clamp recordings in brain slices infected with AAV2/9-eIF4E-eGFP or AAV2/9-eGFP (Fig. S6J). We found that not only the action potentials recorded in current-clamp mode but also the resting potential and input resistance showed no significant difference between the eIF4E group and the eGFP group (Fig. S6K, L). Together, the above results suggest that overexpression of eIF4E in hippocampal neurons of NPSD mice promotes the development of the PSD phenotype without affecting neuronal function.

Downregulation of eIF4E in Hippocampal Neurons Does Not Alter Neuronal Function but Inhibits Microglial Activation and Alleviates the Inflammatory Response in PSD Mice

To demonstrate whether downregulation of eIF4E has an effect on neuronal function, we made patch clamp recordings in brain slices infected with AAV2/9-Si-eIF4E-eGFP or AAV2/9-Scr-eIF4E-eGFP (Fig. 7A). We found that the action potentials recorded in current-clamp mode were similar with no significant difference between the Si-eIF4E and Scr-eIF4E groups, and the analysis of membrane properties also showed no significant difference (Fig. 7B–D). These results suggest that the ameliorative effect of eIF4E on depression-like behavior in PSD mice may not act by directly affecting the function of neurons.

Since neither overexpression nor downregulation of eIF4E altered neuronal function, and the occurrence of PSD is associated with microglial activation [38], to further explore the possible cellular mechanisms by which eIF4E downregulation improves depressive-like behavior in PSD mice, we first observed the morphology and assessed the function of microglia in the hippocampal region of PSD mice. Staining with the microglial marker Iba1 showed that, compared to sham control and NPSD mice, the morphology of microglia in PSD mice displayed a more ramified shape with a larger cell body and markedly shorter and fewer branches (Fig. S7A). To quantify the morphological changes of microglial activation, we reconstructed single microglia cells with overlaid concentric circles (Fig. S7C). Sholl analysis revealed that PSD mice had more $Iba1^+$ cells than sham and NPSD mice (Fig. S7B) and the intersection numbers at 20 or 25 μm from the soma in PSD mice were much fewer than those in sham and NPSD mice (Fig. S7D). Amoeboid microglia are thought to be in an activated state, which causes the release of pro-inflammatory cytokines, leading to neuroinflammation [39, 40]. To test microglial function in PSD mice, we next examined the expression of inflammatory cytokines in the hippocampal tissue by qPCR. Analysis of relative gene expression showed that *IL-1*, *IL-6*, and *TNF-α,* but not *IL-10*, was robustly increased in PSD as compared with sham control or NPSD mice (Fig. S7E).

To demonstrate whether eIF4E affects the activation of microglia in PSD mice, we next used siRNA to downregulate *eIF4E* expression in the hippocampus of PSD mice, and then made observations and analyses of the morphology and function of microglia as above. Both the staining and the reconstruction of single microglial cells showed that si-eIF4E, but not scr-eIF4E, increased the branches and shrank the cell soma of microglia in the hippocampus of PSD mice (Fig. 7E). Sholl analysis demonstrated significant increase of the intersection numbers at 20 or 25 μm from the soma in si-eIF4E-treated PSD mice when compared with PSD or scr-eIF4E-injected PSD mice, and si-eIF4E-treated PSD mice had fewer $Iba1^+$ cells (Fig. 7F). In addition, measurements of relative gene expression showed that *IL-1*, *IL-6*, and *TNF-α,* but not *IL-10*, remarkably decreased in the hippocampus of si-eIF4E-treated PSD mice, rather than scr-eIF4E or PSD mice alone (Fig. 7G). Together, the above results demonstrate that microglia are activated in the hippocampus of PSD mice, while reducing eIF4E reverses the microglial activation and alleviates the neuroinflammation in PSD mice

Discussion

In this study, we used a previously-established mouse model of photothrombosis-induced cortical ischemia [30] and screened the PSD and NPSD phenotypes by multiple post-stroke behavioral tests combined with unsupervised fuzzy cluster analysis. We demonstrated that the screened PSD mice have a typical depression-like behavioral phenotype and that the occurrence rate after stroke is consistent with the epidemiology of clinical PSD. The whole-brain PET scanning and analysis of the screened PSD mice revealed that the hippocampus is the most severely affected brain region secondary to cortical ischemia. Subsequent experiments on the hippocampal transcriptome and bioinformatics analysis revealed that miR-34b-3p is closely associated with the development of PSD. Both target gene prediction and experiments demonstrated that *eIF4E* is the target gene of miR-34b-3p and is expressed in neurons. To our surprise, up- or down-regulation of *eIF4E* does not affect neuronal

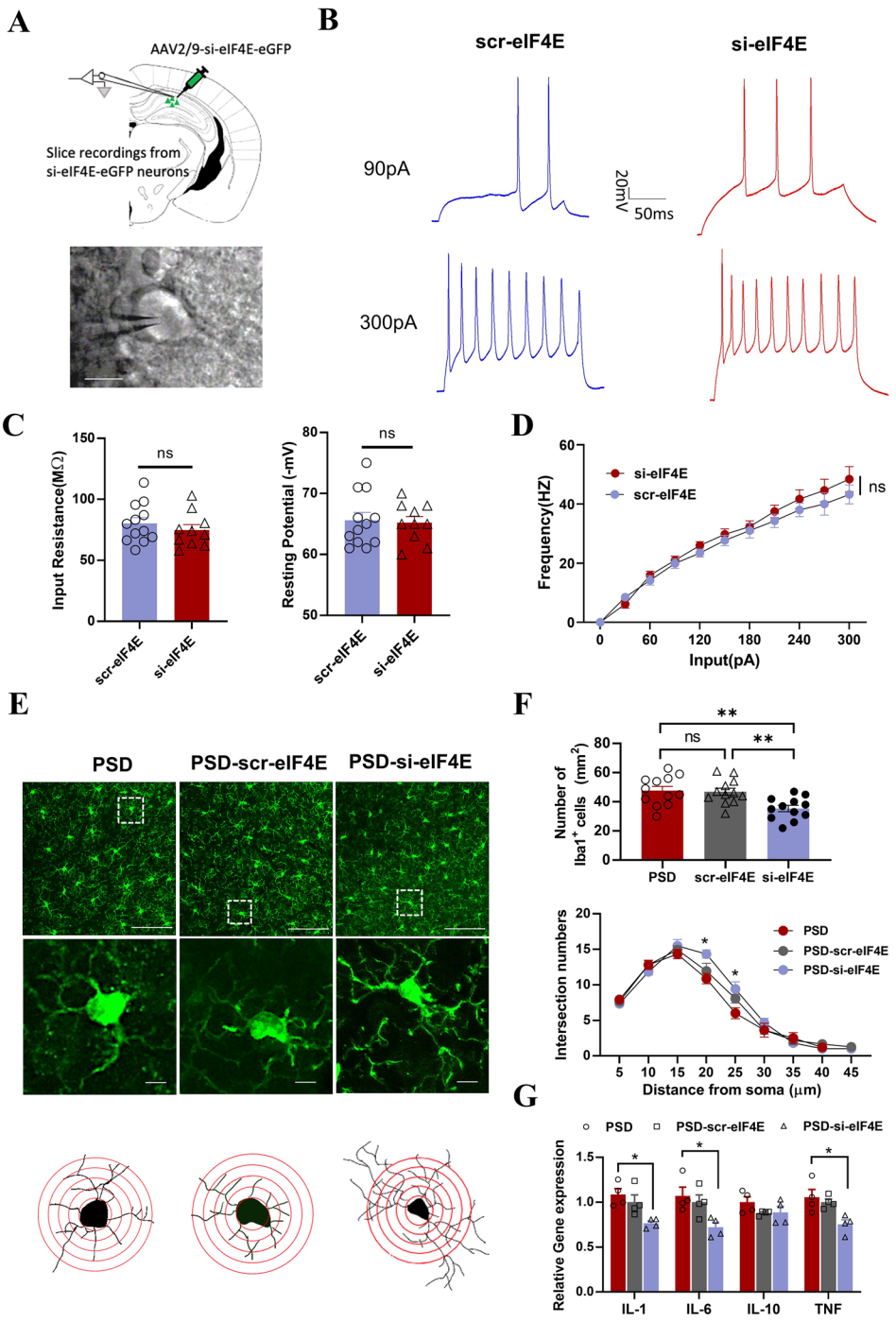

Fig. 7 Downregulation of eIF4E inhibits microglial activation and improves the inflammatory response in PSD mice **A** AAV-si-eIF4E-eGFP was injected into hippocampal pyramidal neurons of PSD mice, and recordings made from GFP$^+$ cells (scale bar, 20 μm). **B** Traces of depolarizing current injections. **C** Bar graph showing the input resistance and resting potential of each group ($n=12$ for PSD-scr-eIF4E and $n=10$ for PSD-si-eIF4E). **D** Frequency of action potentials over a range of current steps ($n=12$ for PSD-scr-eIF4E and $n=10$ for PSD-si-eIF4E, two-way ANOVA). **E** Representative confocal images of immunofluorescence staining with an antibody against Iba1 (green) in the hippocampus of PSD, PSD-scr-eIF4E, and PSD-si-eIF4E mice. Magnified images and typical microglia are shown below each group [scale bars, 50 μm (upper), 5 μm (lower)]. **F** Upper, bar graph showing the number of Iba1$^+$ cells, (PSD *vs* si-eIF4E $^{**}P=0.005$, scr-eIF4E *vs* si-eIF4E $^{**}P=0.0093$, $F=7.324$); lower, analysis of intersection numbers of microglia branches over the distance from soma (at 20 μm $^{*}P=0.0106$, $F=5.102$; at 25 μm $^{*}P=0.0150$ $F=4.672$). ($n=15$ for PSD, $n=16$ for PSD-scr-eIF4E and $n=12$ for PSD-si-eIF4E, one-way ANOVA). **G** Relative gene expression of IL-1, IL-6, IL-10, and TNF in the hippocampus of PSD, PSD-scr-eIF4E, and PSD-si-eIF4E mice ($n=4$ per group, in IL-1 $^{*}P=0.0144$, $F=6.948$; in IL-6 $^{*}P=0.0306$, $F=5.407$; in TNF $^{*}P=0.0195$, $F=6.570$).

function but influences PSD by regulating microglial activation. Thus, our study provides evidence that *eIF4E* can be used as a potential target for the treatment of PSD.

To date, there has been considerable variation in the use of PSD models, such as the selection of stroke models, the observational time of post-stroke behavioral assessment, and the use of behavioral testing methods. Notably, some research groups have reported reliable "depression-like syndromes" characterized by multi-tiered degrees of anxiety, despair, and depression following different middle cerebral artery occlusion or microembolization models [41–47]. Moreover, some studies have even confirmed that stroke-induced psychiatric alterations can be treated with antidepressants [41, 45]. Here, we used our previously-established mouse model of photothrombosis-induced cortical ischemia [30], which allows accurate control of the site and size of ischemic foci. Then, based on the unsupervised fuzzy clustering analysis from Matthew Boyko [28], we successfully

screened PSD mice with typical phenotypes of depression-like behavior, which are consistent with clinical morbidity and improve the predictive effectiveness of experimental stroke studies. Our PSD mouse model will help future research find a way around the translational roadblocks in the development of stroke treatments.

According to clinical studies, the primary lesion in patients with PSD is usually located in the left hemisphere, particularly in the dorsolateral prefrontal cortex [48]. This was the rationale for our PSD model induced by cortical photothrombosis. Interestingly, we found that the hippocampus of PSD mice was the most severely affected region secondary to cortical ischemia. This result is consistent with Sture Liljequist's report on secondary delayed lesions in the hippocampus and thalamus after focal cerebral ischemia induced by extradural compression of a specific area in the somatosensory cortex [49]. In addition, previous studies have also reported post-ischemic hippocampal lesions in global cerebral ischemia [50]. The mechanisms behind these results may lie in the rich, reciprocal fiber projection relationship between the ischemic cortical areas and the hippocampus. When cortical areas are injured first, the hippocampus develops secondary damage due to the loss of structural and functional connections to the cortex [51]. Thus, our study confirmed the existence of a secondary remote brain lesion following a primary ischemic cortical insult, which makes the current PSD model a promising tool for further studies on the underlying neural circuit mechanisms.

Studies have shown that stable expression of miRNA maintains homeostasis and normal neuronal functions, which include neurogenesis, neuronal differentiation, and synaptic plasticity [52]. However, aberrant expression of miRNA is associated with apoptosis of neuronal cells, the inflammatory response, and oxidative stress [53]. A comprehensive analysis by Liang *et al.* showed that certain miRNAs, such as miR-140-5p, could provide early warning for PSD [54]. Moreover, miRNAs may participate in the development and progression of PSD through activation of associated inflammatory cytokines in the brain [55]. For example, rats with stroke treated with miR-363-3p mimics show fewer depressive symptoms and reduced neuro-inflammation [56]. Here, we identified a novel miRNA, miR-34b-3p, by RNA-Seq from the hippocampus of PSD mice. Our study first confirmed that decreased miR-34b-3p in the hippocampus leads to a shift from NPSD to PSD, while overexpression of miR-34b-3p alleviates the depression-like symptoms. The caveat here is that the specificity of brain tissue ensures the credibility of RNA-sequencing analysis, and this will be more profound if relevant results of hippocampal subregions like CA1, CA3, and DG are obtained. Mark *et al.* used next-generation RNA-seq to produce a quantitative, whole-genome characterization of gene expression for the granule cells and mossy cells of the dentate gyrus, and pyramidal cells of areas CA3, CA2, and CA1. They analyzed the transcriptomes of each of these five excitatory populations, which they referred to as five distinct cell "classes". Then they profiled the excitatory cells comprising the trisynaptic loop at the dorsal and ventral poles of the hippocampus and referred to cell classes at opposite poles to be from distinct regions [57]. In addition, Sheel *et al.* discovered that distinct subregions within CA1 and CA3 are composed of unique combinations of cells in different transcriptional states [58]. We intend to perform single-cell spatiotemporal transcriptome sequencing to further explore the cellular and molecular mechanisms of PSD regarding different types of neurons in different subregions of the hippocampus.

We further confirmed that *eIF4E* is the target gene of miR-34b-3p, and inhibition of eIF4E expression in hippocampal neurons improves depression-like behaviors in PSD mice. It is known that eIF4E is the cap-binding protein that binds to mRNA, allowing the recruitment of ribosomes and translation initiation [59]. Recent studies have highlighted the importance of eIF4E in the brain. For example, eIF4E-dependent translation is essential for neuronal cell function and its aberrant function has been implicated in neurodevelopmental and neuropsychiatric conditions [60]. The mechanism of eIF4E's role in the brain is considered to be linked to cell-cycle progression, cell survival, and cell motility [61, 62], as well as inflammation and immunity [63, 64]. Our findings differ from these in that neither overexpression nor knockdown of eIF4E in hippocampal neurons affected neuronal function, but rather activated microglia and promoted neuro-inflammation. We speculate that eIF4E may regulate the transcription of certain genes that encode proteins like the cytokines S1P, LPS, HMGB1, S100B, and CKLF1. These factors are released from neurons and bind to microglial cell membrane receptors, such as the cytokine receptors S1PR, RAGE, TLR4, IL-4R, and CCR4, to trigger pro-inflammatory cellular signaling pathways [65]. In addition, the previous studies differ from ours in that they found that a decrease of *p*-eIF4E or the *eIF4E* gene in whole brain is associated with major depression, and we discovered an increase in total eIF4E in the hippocampal neurons involved in post-stroke depression. Thus, the gene expression, modification of eIF4E, and distribution in different brain regions, may play different roles in the development of different models of depression. For example, studies have also shown that eIF4E serves as the point of signal integration for the convergence of the ERK–MEK and PI3K–Akt–mTOR pathways. Increasing eIF4F complex availability *via* the genetic elimination of 4E-BP2 can enhance the degree of depression [66]. Therefore, we believe that eIF4E is like a "double-edged sword". Excessive expression of eIF4E in specific brain regions may also lead to psychiatric disorders by promoting gene transcription or crosstalk with glial cells. Even so, how

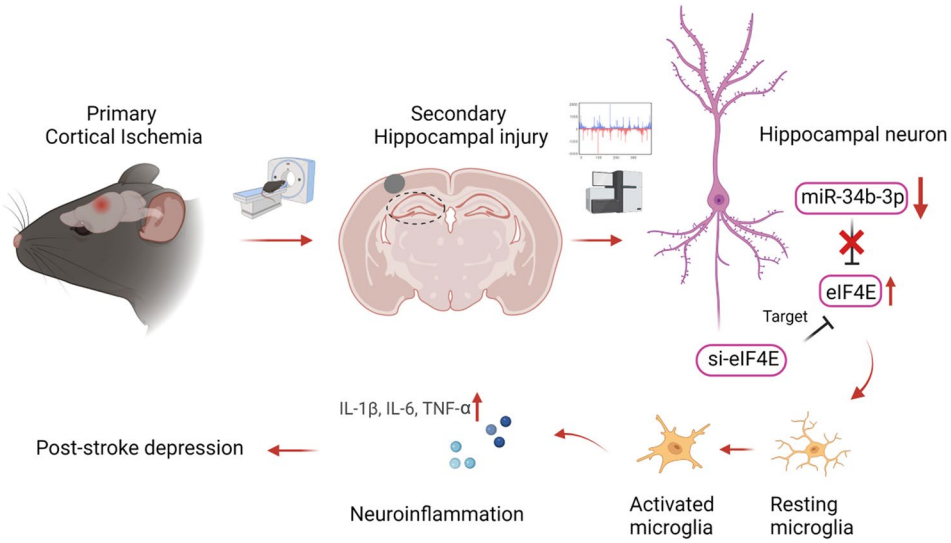

Fig. 8 Summary cartoon. Primary cortical ischemia induces secondary hippocampal injury and downregulates neuronal miR34b-3p, which leads to increased expression of its target gene *eIF4E*. Upregulation of eIF4E causes neuroinflammation through an indirect pathway of microglial activation. However, inhibition of eIF4E in hippocampal neurons alleviates neuroinflammation and ameliorates the symptoms of PSD.

eIF4E in neurons affects microglial function requires further studies, but our study still provides evidence for considering eIF4E as a potential target to treat PSD.

Conclusion

In conclusion, our study using comprehensive approaches screened PSD mice with a typical depression-like behavioral phenotype that is consistent with clinical PSD morbidity. We found that downregulation of miR-34b-3p and upregulation of its target gene *eIF4E* caused PSD development through the activation of microglia, without affecting neuronal functions (Fig. 8). However, how the miR-34b-3p–eIF4E signaling axis in neurons affects microglial activation requires future studies to elucidate the specific cellular and molecular mechanisms. More precise and targeted therapies focusing on genetic and protein functional aberrations are needed to investigate and abolish PSD and its long-term outcomes.

Acknowledgements We would like to thank Dr. Daniel Fulton from the University of Birmingham for English language editing. Figures were created with BioRender.com. This work was supported by the National Natural Science Foundation of China (81870932, 81571078, 51627807, 31721002, 81920208014, and 31930051) and China Postdoctoral Science Foundation Funded Project (2020M672324, 2020TQ0113).

Conflict of interest The authors declare that they have no conflicts of interest.

References

1. Flaster M, Sharma A, Rao M. Poststroke depression: A review emphasizing the role of prophylactic treatment and synergy with treatment for motor recovery. Top Stroke Rehabil 2013, 20: 139–150.
2. Perahia DGS, Quail D, Desaiah D, Montejo AL, Schatzberg AF. Switching to duloxetine in selective serotonin reuptake inhibitor non- and partial-responders: Effects on painful physical symptoms of depression. J Psychiatr Res 2009, 43: 512–518.
3. Willner P, Scheel-Krüger J, Belzung C. The neurobiology of depression and antidepressant action. Neurosci Biobehav Rev 2013, 37: 2331–2371.
4. Robinson RG, Jorge RE. Post-Stroke Depression: A Review. Am J Psychiatry 2016, 173: 221–231.
5. Whyte EM, Mulsant BH, Vanderbilt J, Dodge HH, Ganguli M. Depression after stroke: a prospective epidemiological study. J Am Geriatr Soc 2004, 52: 774–778.
6. Whyte EM, Mulsant BH. Post stroke depression: Epidemiology, pathophysiology, and biological treatment. Biol Psychiatry 2002, 52: 253–264.
7. Aström M, Adolfsson R, Asplund K. Major depression in stroke patients. A 3-year longitudinal study. Stroke 1993, 24: 976–982.
8. Almhdawi KA, Alazrai A, Kanaan S, Shyyab AA, Oteir AO, Mansour ZM. Post-stroke depression, anxiety, and stress symptoms and their associated factors: A cross-sectional study. Neuropsychol Rehabil 2021, 31: 1091–1104.
9. Alghwiri AA. The Correlation between Depression, Balance, and Physical Functioning Post Stroke. J Stroke Cerebrovasc Dis 2016, 25: 475–479.
10. Ayasrah SM, Ahmad MM, Basheti IA. Post-Stroke Depression in Jordan: Prevalence Correlates and Predictors. J Stroke Cerebrovasc Dis 2018, 27: 1134–1142.
11. Al Qawasmeh M, Aldabbour B, Abuabada A, Abdelrahman K, Elamassie S, Khweileh M, *et al*. Prevalence, Severity, and Predictors of Poststroke Depression in a Prospective Cohort of Jordanian Patients. Stroke Res Treat 2022, 2022: 6506326.
12. Perrain R, Calvet D, Guiraud V, Mekaoui L, Mas JL, Gorwood P. Depressive-, Cognitive- or Stroke-Related Risk Factors of Post-Stroke Depression: Which One Could Better Help Clinicians and Patients? Neuropsychiatr Dis Treat 2021, 17: 1243–1251.
13. Villa RF, Ferrari F, Moretti A. Post-stroke depression: Mechanisms and pharmacological treatment. Pharmacol Ther 2018, 184: 131–144.
14. Wei N, Yong W, Li XY, Zhou YF, Deng MF, Zhu HZ, *et al*. Post-stroke depression and lesion location: A systematic review. J Neurol 2015, 262: 81–90.

15. Provinciali L, Coccia M. Post-stroke and vascular depression: a critical review. Neurol Sci 2002, 22: 417–428.
16. Kim JM, Stewart R, Bae KY, Kim SW, Kang HJ, Shin IS, *et al*. Serotonergic and BDNF genes and risk of depression after stroke. J Affect Disord 2012, 136: 833–840.
17. Sanacora G, Treccani G, Popoli M. Towards a glutamate hypothesis of depression: An emerging frontier of neuropsychopharmacology for mood disorders. Neuropharmacology 2012, 62: 63–77.
18. Hannestad J, DellaGioia N, Bloch M. The effect of antidepressant medication treatment on serum levels of inflammatory cytokines: A meta-analysis. Neuropsychopharmacology 2011, 36: 2452–2459.
19. Vasudeva K, Munshi A. miRNA dysregulation in ischaemic stroke: Focus on diagnosis, prognosis, therapeutic and protective biomarkers. Eur J Neurosci 2020, 52: 3610–3627.
20. He WZ, Chen SQ, Chen XG, Li SX, Chen WJ. Bioinformatic Analysis of Potential microRNAs in Ischemic Stroke. J Stroke Cerebrovasc Dis 2016, 25: 1753–1759.
21. Bartel DP. MicroRNAs: genomics, biogenesis, mechanism, and function. Cell 2004, 116: 281–297.
22. Flynt AS, Lai EC. Biological principles of microRNA-mediated regulation: Shared themes amid diversity. Nat Rev Genet 2008, 9: 831–842.
23. Mohr AM, Mott JL. Overview of microRNA biology. Semin Liver Dis 2015, 35: 3–11.
24. Giridharan VV, Thandavarayan RA, Fries GR, Walss-Bass C, Barichello T, Justice NJ, *et al*. Newer insights into the role of miRNA a tiny genetic tool in psychiatric disorders: Focus on post-traumatic stress disorder. Transl Psychiatry 2016, 6: e954.
25. Wu JH, Wu ZZ, He AD, Zhang TM, Zhang P, Jin J, *et al*. Genome-Wide Screen and Validation of Microglia Pro-Inflammatory Mediators in Stroke. Aging Dis 2021, 12: 786–800.
26. Cai Y, Zhang YF, Ke X, Guo Y, Yao CY, Tang N, *et al*. Transcriptome Sequencing Unravels Potential Biomarkers at Different Stages of Cerebral Ischemic Stroke. Front Genet 2019, 10: 814.
27. Labat-gest V, Tomasi S. Photothrombotic ischemia: a minimally invasive and reproducible photochemical cortical lesion model for mouse stroke studies. J Vis Exp 2013: 50370.
28. Ifergane G, Boyko M, Frank D, Shiyntum HN, Grinshpun J, Kuts R, *et al*. Biological and Behavioral Patterns of Post-Stroke Depression in Rats. Can J Neurol Sci 2018, 45: 451–461.
29. Guo Y, Li H, Ke X, Deng MF, Wu ZZ, Cai Y, *et al*. Degradation of Caytaxin Causes Learning and Memory Deficits *via* Activation of $DAPK_1$ in Aging. Mol Neurobiol 2019, 56: 3368–3379.
30. Jin HJ, Pei L, Li YN, Zheng H, Yang S, Wan Y, *et al*. Alleviative effects of fluoxetine on depressive-like behaviors by epigenetic regulation of *BDNF* gene transcription in mouse model of post-stroke depression. Sci Rep 2017, 7: 14926.
31. Amorim IS, Kedia S, Kouloulia S, Simbriger K, Gantois I, Jafarnejad SM, *et al*. Loss of eIF4E Phosphorylation Engenders Depression-like Behaviors *via* Selective mRNA Translation. J Neurosci 2018, 38: 2118–2133.
32. Friedländer MR, Mackowiak SD, Li N, Chen W, Rajewsky N. miRDeep2 accurately identifies known and hundreds of novel microRNA genes in seven animal clades. Nucleic Acids Res 2012, 40: 37–52.
33. Love MI, Huber W, Anders S. Moderated estimation of fold change and dispersion for RNA-seq data with DESeq2. Genome Biol 2014, 15: 550.
34. Ji ZY, Li H, Yang Z, Huang X, Ke X, Ma SH, *et al*. Kibra Modulates Learning and Memory *via* Binding to Dendrin. Cell Rep 2019, 26: 2064-2077.e7.
35. Li XY, Chen WT, Pan K, Li H, Pang P, Guo Y, *et al*. Serotonin receptor 2c-expressing cells in the ventral CA1 control attention *via* innervation of the Edinger-Westphal nucleus. Nat Neurosci 2018, 21: 1239–1250.
36. Yang Y, Shu XG, Liu D, Shang Y, Wu Y, Pei L, *et al*. EPAC null mutation impairs learning and social interactions *via* aberrant regulation of miR-124 and Zif268 translation. Neuron 2012, 73: 774–788.
37. Ma XY, Xiao WC, Li H, Pang P, Xue FX, Wan L, *et al*. Metformin restores hippocampal neurogenesis and learning and memory *via* regulating gut microbiota in the obese mouse model. Brain Behav Immun 2021, 95: 68–83.
38. Nagy EE, Frigy A, Szász JA, Horváth E. Neuroinflammation and microglia/macrophage phenotype modulate the molecular background of post-stroke depression: A literature review. Exp Ther Med 2020, 20: 2510–2523.
39. Voet S, Prinz M, van Loo G. Microglia in Central Nervous System Inflammation and Multiple Sclerosis Pathology. Trends Mol Med 2019, 25: 112–123.
40. Tang Y, Le WD. Differential Roles of M1 and M2 Microglia in Neurodegenerative Diseases. Mol Neurobiol 2016, 53: 1181–1194.
41. Kato M, Iwata H, Okamoto M, Ishii T, Narita H. Focal cerebral ischemia-induced escape deficit in rats is ameliorated by a reversible inhibitor of monoamine oxidase-A: Implications for a novel animal model of post-stroke depression. Biol Pharm Bull 2000, 23: 406–410.
42. Winter B, Juckel G, Viktorov I, Katchanov J, Gietz A, Sohr R, *et al*. Anxious and hyperactive phenotype following brief ischemic episodes in mice. Biol Psychiatry 2005, 57: 1166–1175.
43. Craft TKS, DeVries AC. Role of IL-1 in poststroke depressive-like behavior in mice. Biol Psychiatry 2006, 60: 812–818.
44. Royl G, Balkaya M, Lehmann S, Lehnardt S, Stohlmann K, Lindauer U, *et al*. Effects of the PDE5-inhibitor vardenafil in a mouse stroke model. Brain Res 2009, 1265: 148–157.
45. Kronenberg G, Balkaya M, Prinz V, Gertz K, Ji SB, Kirste I, *et al*. Exofocal Dopaminergic Degeneration as Antidepressant Target in Mouse Model of Poststroke Depression. Biol Psychiatry 2012, 72: 273–281.
46. Nemeth N, Kiss F, Hever T, Brath E, Sajtos E, Furka I, *et al*. Hemorheological consequences of hind limb ischemia-reperfusion differs in normal and gonadectomized male and female rats. Clin Hemorheol Microcirc 2012, 50: 197–211.
47. Boyko M, Kutz R, Gruenbaum BF, Cohen H, Kozlovsky N, Gruenbaum SE, *et al*. The influence of aging on poststroke depression using a rat model *via* middle cerebral artery occlusion. Cogn Affect Behav Neurosci 2013, 13: 847–859.
48. Grajny K, Pyata H, Spiegel K, Lacey EH, Xing SH, Brophy C, *et al*. Depression Symptoms in Chronic Left Hemisphere Stroke Are Related to Dorsolateral Prefrontal Cortex Damage. J Neuropsychiatry Clin Neurosci 2016, 28: 292–298.
49. Holmberg P, Liljequist S, Wägner A. Secondary brain injuries in thalamus and *hippocampus* after focal ischemia caused by mild, transient extradural compression of the somatosensori cortex in the rat. Curr Neurovasc Res 2009, 6: 1–11.
50. Johansen FF, Zimmer J, Diemer NH. Early loss of somatostatin neurons in dentate hilus after cerebral ischemia in the rat precedes CA-1 pyramidal cell loss. Acta Neuropathol 1987, 73: 110–114.
51. Ke X, Ma SH, Zhang YF, Yi Y, Yu HY, Yu D, *et al*. Death-associated Protein Kinase 1 Impairs the hippocampo-prefrontal Cortical Circuit and Mediates Post-stroke Depression. Explor Res Hypothesis Med 2018, 3: 1–5.
52. Yin KJ, Deng Z, Huang HR, Hamblin M, Xie CQ, Zhang JF, *et al*. miR-497 regulates neuronal death in mouse brain after transient focal cerebral ischemia. Neurobiol Dis 2010, 38: 17–26.
53. Reddy MA, Jin W, Villeneuve L, Wang M, Lanting LD, Todorov I, *et al*. Pro-inflammatory role of microrna-200 in vascular smooth muscle cells from diabetic mice. Arterioscler Thromb Vasc Biol 2012, 32: 721–729.

54. Baccaro A, Wang YP, Brunoni AR, Candido M, Conforto AB, da Costa Leite C, *et al*. Does stroke laterality predict major depression and cognitive impairment after stroke? Two-year prospective evaluation in the EMMA study. Prog Neuropsychopharmacol Biol Psychiatry 2019, 94: 109639.
55. Witwer KW, Sisk JM, Gama L, Clements JE. MicroRNA regulation of IFN-β protein expression: rapid and sensitive modulation of the innate immune response. J Immunol 2010, 184: 2369–2376.
56. Lisanby SH. Electroconvulsive therapy for depression. N Engl J Med 2007, 357: 1939–1945.
57. Cembrowski MS, Wang LH, Sugino K, Shields BC, Spruston N. Hipposeq: a comprehensive RNA-seq database of gene expression in hippocampal principal neurons. Elife 2016, 5: e14997.
58. Shah S, Lubeck E, Zhou W, Cai L. *In Situ* Transcription Profiling of Single Cells Reveals Spatial Organization of Cells in the Mouse hippocampus. Neuron 2016, 92: 342–357.
59. Amorim IS, Lach G, Gkogkas CG. The Role of the Eukaryotic Translation Initiation Factor 4E (eIF4E) in Neuropsychiatric Disorders. Front Genet 2018, 9: 561.
60. Costa-Mattioli M, Monteggia LM. mTOR complexes in neurodevelopmental and neuropsychiatric disorders. Nat Neurosci 2013, 16: 1537–1543.
61. Rhoads RE, Joshi-Barve S, Rinker-Schaeffer C. Mechanism of action and regulation of protein synthesis initiation factor 4E: Effects on mRNA discrimination, cellular growth rate, and oncogenesis. Prog Nucleic Acid Res Mol Biol 1993, 46: 183–219.
62. Steinberger J, Chu J, Maïga RI, Sleiman K, Pelletier J. Developing anti-neoplastic biotherapeutics against eIF4F. Cell Mol Life Sci 2017, 74: 1681–1692.
63. Hoang HD, Graber TE, Alain T. Battling for Ribosomes: Translational Control at the Forefront of the Antiviral Response. J Mol Biol 2018, 430: 1965–1992.
64. Wang S, He HH, Long JH, Sui X, Yang J, Lin GD, *et al*. $TRPV_4$ Regulates Soman-Induced Status Epilepticus and Secondary Brain Injury *via* NMDA Receptor and NLRP3 Inflammasome. Neurosci Bull 2021, 37: 905–920.
65. Jiang CT, Wu WF, Deng YH, Ge JW. Modulators of microglia activation and polarization in ischemic stroke (Review). Mol Med Rep 2020, 21: 2006–2018.
66. Banko JL, Hou LF, Poulin F, Sonenberg N, Klann E. Regulation of eukaryotic initiation factor 4E by converging signaling pathways during metabotropic glutamate receptor-dependent long-term depression. J Neurosci 2006, 26: 2167–2173.